Editors' Suggestion

Spin-Dependent $\pi\pi^*$ Gap in Graphene on a Magnetic Substrate

P. M. Sheverdyaeva,[1,*] G. Bihlmayer,[2] E. Cappelluti,[1] D. Pacilé,[3] F. Mazzola,[4,5] N. Atodiresei,[2] M. Jugovac,[6] I. Grimaldi,[3] G. Contini,[7] Asish K. Kundu,[1,8,9] I. Vobornik,[5] J. Fujii,[5] P. Moras,[1] C. Carbone,[1] and L. Ferrari[7,†]

[1]*CNR-Istituto di Struttura della Materia (CNR-ISM), Strada Statale 14, km 163.5, 34149 Trieste, Italy*
[2]*Peter Grünberg Institut and Institute for Advanced Simulation, Forschungszentrum Jülich and JARA, 52425 Jülich, Germany*
[3]*Dipartimento di Fisica, Università della Calabria, 87036 Arcavacata di Rende (CS), Italy*
[4]*Department of Molecular Sciences and Nanosystems, Ca' Foscari University of Venice, 30172 Venice, Italy*
[5]*CNR-Istituto Officina dei Materiali (CNR-IOM), Strada Statale 14, km 163.5, 34149 Trieste, Italy*
[6]*Elettra Sincrotrone Trieste, Strada Statale 14 km 163.5, 34149 Trieste, Italy*
[7]*CNR-Istituto di Struttura della Materia (CNR-ISM), Via del Fosso del Cavaliere 100, 00133 Roma, Italy*
[8]*International Center for Theoretical Physics (ICTP), Trieste 34151, Italy*
[9]*National Synchrotron Light Source II, Brookhaven National Laboratory, Upton, New York 11973, USA*

(Received 1 December 2023; revised 6 March 2024; accepted 21 May 2024; published 28 June 2024)

We present a detailed analysis of the electronic properties of graphene/Eu/Ni(111). By using angle- and spin-resolved photoemission spectroscopy and *ab initio* calculations, we show that the intercalation of Eu in the graphene/Ni(111) interface gives rise to a gapped freestanding dispersion of the $\pi\pi^*$ Dirac cones at the $\bar{\mathrm{K}}$ point with an additional lifting of the spin degeneracy due to the mixing of graphene and Eu states. The interaction with the magnetic substrate results in a large spin-dependent gap in the Dirac cones with a topological nature characterized by a large Berry curvature and a spin-polarized Van Hove singularity, whose closeness to the Fermi level gives rise to a polaronic band.

DOI: 10.1103/PhysRevLett.132.266401

Graphene is a highly promising material for spintronics applications due to its large spin transport coherence length [1,2] and its particular band structure, especially for the massless Dirac cones and the nearly flat Van Hove singularities (VHSs) [3–7]. Despite graphene being a nonmagnetic material, it can acquire spin polarization by the proximity effect in contact with magnetic materials. However, on transition metals Fe, Co, and Ni the interaction with $3d$ states strongly modifies the $\pi\pi^*$ states, which form complex hybrid bands and lose their linear character [8–11]. One of the goals of spintronics would be turning graphene into a spin conductor, finding supporting magnetic materials that preserve the graphene electronic properties almost unaltered [5–7,12]. Removing the spin degeneracy may turn graphene into a spin field effect transistor [13], spin valve [14], or spin-transfer torque device [15]. In turn, a spin-polarized VHS may lead to unconventional superconductivity [16], quantum phases [17], and insulating topological states [18,19].

Recent works have addressed the intercalation in graphene-ferromagnet heterostructures [9,19–27], where the π and π^* bands recover their characteristic linearity. In particular, the rare earth metallic intercalants additionally induce a heavy electron doping that brings the VHS to the proximity of the Fermi level (FL) [19–21]. A remarkable example is the Eu intercalated graphene/Ni(111) system, which has been studied by density functional theory (DFT) calculations and x-ray magnetic circular dichroism (XMCD) [21]. The calculations show that the $2p$ states of C atoms lose the characteristic hybridization with the $3d$ states of Ni. The electron density of states is spin dependent and the XMCD data show that the Eu monolayer is ferromagnetic within the layer while being antiferromagnetically coupled to the Ni underlayer. The presence of the Ni film leads to a magnetic ordering above room temperature in the Eu layer, in contrast to the case of an iridium substrate that leads to a much lower transition temperature [28]. This makes the graphene/Eu/Ni(111) system interesting for possible applications in spintronics.

In this Letter, we investigate the electronic and magnetic properties of graphene/Eu/Ni(111), by angle- and spin-resolved photoemission spectroscopy (ARPES and spin-ARPES) and DFT calculations. Our results show that, as a consequence of the intercalation, graphene is decoupled from Ni, and its $\pi\pi^*$ states recover a linear dispersion in the proximity of the $\bar{\mathrm{K}}$ point. The interaction with the Eu $4f$ states removes the spin degeneracy near the Dirac point and induces a large spin-dependent gap between the π and π^* bands. The large Eu-induced n doping leads to the emergence of a spin-polarized VHS at FL and a pronounced quasiparticle band. In the vicinity of the energy gap, our calculations suggest the presence of a large Berry curvature, corroborating the topological nature of the bands [29,30].

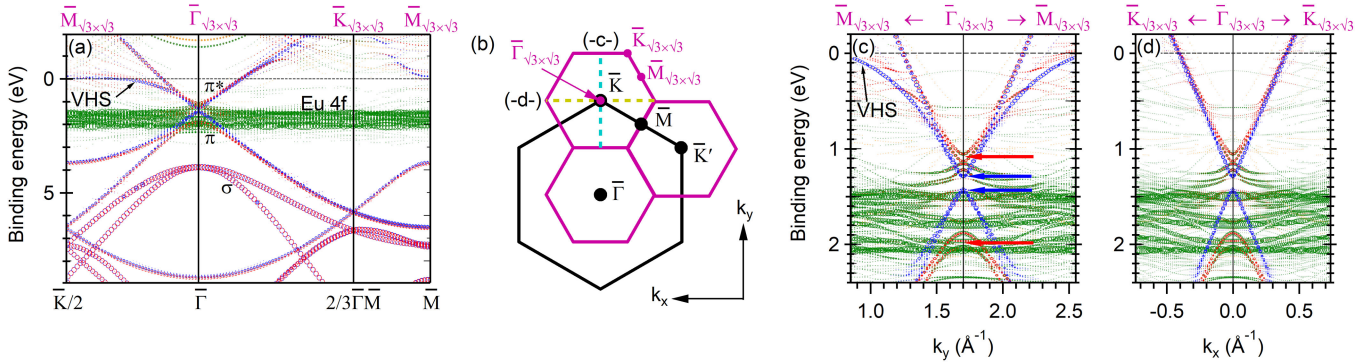

FIG. 1. (a) Spin-resolved DFT band structure calculated for graphene/Eu/Ni(111) along the main high symmetry directions. The red (blue) color indicates the graphene minority (majority) bands. The green (yellow) color indicates the Eu minority (majority) spin channels. The weight of the Ni states, in the background, is artificially reduced for clarity. (b) Schematic of the surface Brillouin zones of the (1×1) graphene/Ni(111) (black) and the $(\sqrt{3} \times \sqrt{3})R30°$ superstructure (magenta). The two segments, investigated by theory and experiment, are drawn in yellow and light blue colors. (c),(d) Enlargement of the calculated bands along $\bar{\Gamma}\bar{K}$ and $p(\bar{\Gamma}\bar{K})$, respectively. Red (blue) arrows indicate the minority (majority) cones. The binding energy scale is referred to FL.

Figure 1(a) shows the calculated band structure of graphene/Eu/Ni(111) (for details see Sec. I of Supplemental Material [31]). The system forms a $(\sqrt{3} \times \sqrt{3})R30°$ superstructure with respect to the pristine graphene and Ni(111) lattices [21]. Its bands are folded as indicated in Fig. 1(b) and by the x axis labels of Fig. 1(a). Since the superlattice-related replicas are not experimentally observed in our photoemission study, due to a weakening of the scattering potential after the intercalation [11,19,53], we will not consider the folding-induced bands and will refer to the (1×1) surface for the indexing. The graphene's $\pi\pi^*$ bands are shifted to higher binding energy with respect to freestanding graphene [see Fig. S1(b) of Supplemental Material Sec. I [31]], due to the electron doping from Eu. The position of the Dirac cone overlaps with the Eu $4f$ minority states shown by green color (Fig. 1). The magnitude of the doping-induced shift (1.4 eV approximately) is similar to the one observed in other graphene systems doped with rare earth or alkaline metals [4,54–57].

Figures 1(c) and 1(d) show an enlargement of the region of the Dirac point along $\bar{\Gamma}\bar{K}$ (k_y) and the perpendicular direction, $p(\bar{\Gamma}\bar{K})$ (k_x), respectively, indicated in Fig. 1(b), revealing several important details in the graphene band structure. First, the $\pi\pi^*$ bands exhibit close to $\bar{K}$ a conical dispersion, typical of a gapped quasifreestanding graphene [9,58,59], indicating that the Eu intercalation attenuates the graphene-Ni interaction. Second, the graphene states acquire a spin polarization in some defined binding energy and wave vector regions where they interact with the Eu states. A large gap of about 900 meV opens for the spin-minority channel, mostly due to the hybridization with the polarized Eu $4f$ states (see Supplemental Material Sec. I [31]). For the majority-spin states, which are not affected by the interaction with the Eu $4f$, the gap is about 150 meV. Furthermore, we notice in the $\bar{\Gamma}\bar{K}$ direction a strong bending of the Dirac π^* band [Fig. 1(a)]. Such flat dispersion is related to the presence of the VHS at the $\bar{M}$ point, which is shifted close to the FL because of the large electron doping [Figs. S1(b) and S1(c) of Supplemental Material Sec. I [31]]. The interaction with the spin-polarized Eu sp bands is expected to induce a spin polarization also for the π^* bands associated with the VHS. This is clearly seen in Fig. S1(c) of Supplemental Material [31], which shows the calculated band structures of graphene on Eu without the Ni substrate, where the VHS shows two spin-split branches. On a Ni substrate, the indirect interaction with Ni states leads to a stronger delocalization of the VHS's minority-spin branch, so only the majority branch can be observed [see Figs. S2(a) and S2(b) of Supplemental Material Sec. I [31] for the corresponding densities of states]. Similar results on the VHS properties were recently reported for the graphene/Eu/Co(0001) [19].

ARPES and spin-ARPES measurements were performed in order to confirm the dispersion and spin-polarization of the graphene $\pi\pi^*$ bands, in particular, near the Dirac point, predicted by the theoretical calculations (for details see Sec. II of Supplemental Material [31]). Figures 2(a) and 2(b) show the ARPES data of the system close to $\bar{K}$ along k_y and k_x, respectively, that can be compared to Figs. 1(c) and 1(d). Dispersing graphene bands are crossed by a broad flat Eu $4f$ state close to 1.5 eV. We can confirm the effects of doping and an almost linear dispersion of the $\pi\pi^*$ bands (see also Fig. S4 of Supplemental Material Sec. II [31]). The second derivative spectra more clearly indicate the presence of two conelike features and the opening of two different energy gaps at the $\bar{K}$ point [Figs. 2(c) and 2(d)], which amount to 250 ± 50 meV (blue arrows) and 1100 ± 50 meV (red arrows). Figure 2(e) reports the spin-integrated energy distribution curves (EDCs) extracted from the $p(\bar{\Gamma}\bar{K})$ map, where it is possible to follow the

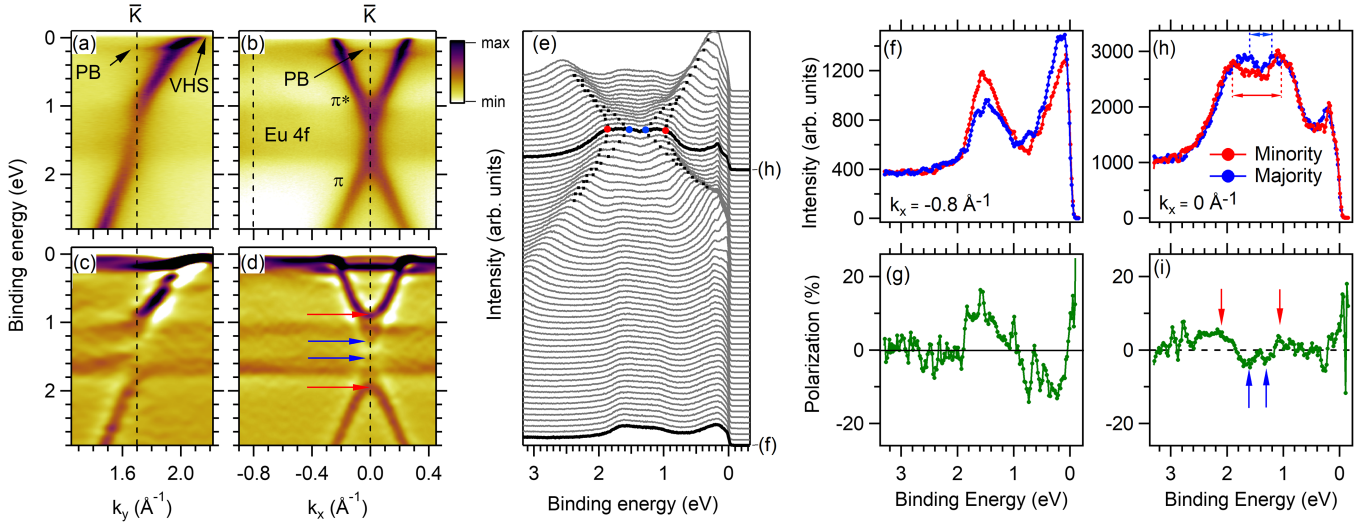

FIG. 2. (a)–(d) Spin-integrated ARPES maps of graphene/Eu/Ni(111) (a),(c) along the $\bar{\Gamma}\,\bar{\mathrm{K}}$ direction and (b),(d) along the $p(\bar{\Gamma}\,\bar{\mathrm{K}})$ directions. (a),(b) As-taken data and (c),(d) their second derivative along the energy axis. (e) EDC spectra extracted from the map shown in (b). Black dots follow the dispersion of the π and π^* states for the two spin channels. The bolded lines correspond to $k_x = 0$ and $k_x = -0.8$ Å^{-1}. Red (blue) dots indicate the edges of the minority (majority) gap. The nondispersive peak at 180 meV of binding energy is the PB. (f),(h) Minority-spin (red curves) and majority-spin (blue curves) EDCs at (f) $k_x = -0.8$ Å^{-1} and (h) $k_x = 0$ Å^{-1} [as the dashed lines indicate in (b)]. Red (blue) arrows indicate the width of the minority (majority) gap. (g),(i) Spin polarizations corresponding to the spectra shown in (f),(h), respectively. Data were acquired at 25 K and a photon energy of 50 eV.

dispersion of the $\pi\pi^*$ states for the two spin channels. These results are in agreement with the DFT predictions for two spin-dependent gaps, which we further confirm by spin-ARPES measurements. We analyzed the spin polarization at two different wave vectors: away from the Dirac point, where only the Eu $4f$ states are visible ($k_x = -0.8$ Å^{-1}), and at the Dirac point ($k_x = 0$ Å^{-1}), where Eu and graphene states overlap [black dashed lines in Fig. 2(b)]. Figures 2(f)–2(i) show the corresponding majority and minority intensities [Figs. 2(f) and 2(h)] and spin-polarization curves [Figs. 2(g) and 2(i)]. Away from the $\bar{\mathrm{K}}$ point, we confirm the spin polarization of the Eu $4f$ states: the majority and minority states of Eu (at ∼1.5 eV) show two similar large single-peak energy profiles with a noncomplete spin polarization of about 15%, due to the finite temperature and a noncomplete magnetic saturation of the sample [Figs. 2(f) and 2(g)]. The sharp peaks just below FL are the Ni states with prevalent polarization opposite to the Eu $4f$ states. At the $\bar{\mathrm{K}}$ point, the majority- and minority-spin states show two-peaked profiles with clearly different energy distances between the peaks [Fig. 2(h)]. We can distinguish the corresponding minima and maxima in the spin-polarization spectra [Fig. 2(i)], better visible for π states, and estimate the peak separation to be about (400 ± 100) meV for the majority-spin channel and (1050 ± 100) meV for the minority-spin channel. These results are in agreement with the majority and minority gap values provided by our calculations.

Close to the FL we can notice in Figs. 2(a) and 2(c) a strong bending of the π^* band with increasing the k_y values (toward the $\bar{\mathrm{M}}$ point). Such feature is in very good agreement with the DFT calculations that predict the VHS of the π^* band to be located just above FL [4,19,60]. Figures 3(a) and 3(b) show the experimental Fermi surface where the VHS is marked by black arrows. In the ARPES maps [Figs. 3(c) and 3(d)] it can be observed as a weak intensity right at FL that extends toward the $\bar{\mathrm{M}}$ point. Because of the low intensity of the VHS, we were not able to access experimentally its spin polarization. The agreement between the DFT calculations and our ARPES and spin-ARPES data for the Dirac cone suggests that the VHS preserves a spin polarization with minority character, similar to the graphene/Eu/Co system [19].

In Figs. 2(a)–2(e) we can also notice a second low-dispersive feature, which stems from the Dirac cone at about 180 meV of binding energy. We identify the nature of this spectral feature as related to polaronic effects, and we denote it as the polaronic band (PB). Such spectral feature, which is also clearly visible in Figs. 3(c)–3(f), is absent in the DFT simulations. We can observe that it extends toward $\bar{\mathrm{M}}$ as a replica of the VHS in Fig. 3(c). A kink at a similar binding energy is commonly observed in graphene bands and is attributed to electron-phonon (e-ph) coupling [58,61–63]. While a band similar to PB is observed on highly n-doped graphenes close to $\bar{\mathrm{M}}$, it is rarely reported at $\bar{\mathrm{K}}$ [4,19,56,64,65] and often attributed to the substrate or dopants [19,64,65]. This hypothesis is in contrast to the variety of systems where this band was observed. The 180 meV binding energy corresponds to the phonon mode of graphene, and indeed several studies associated the PB to

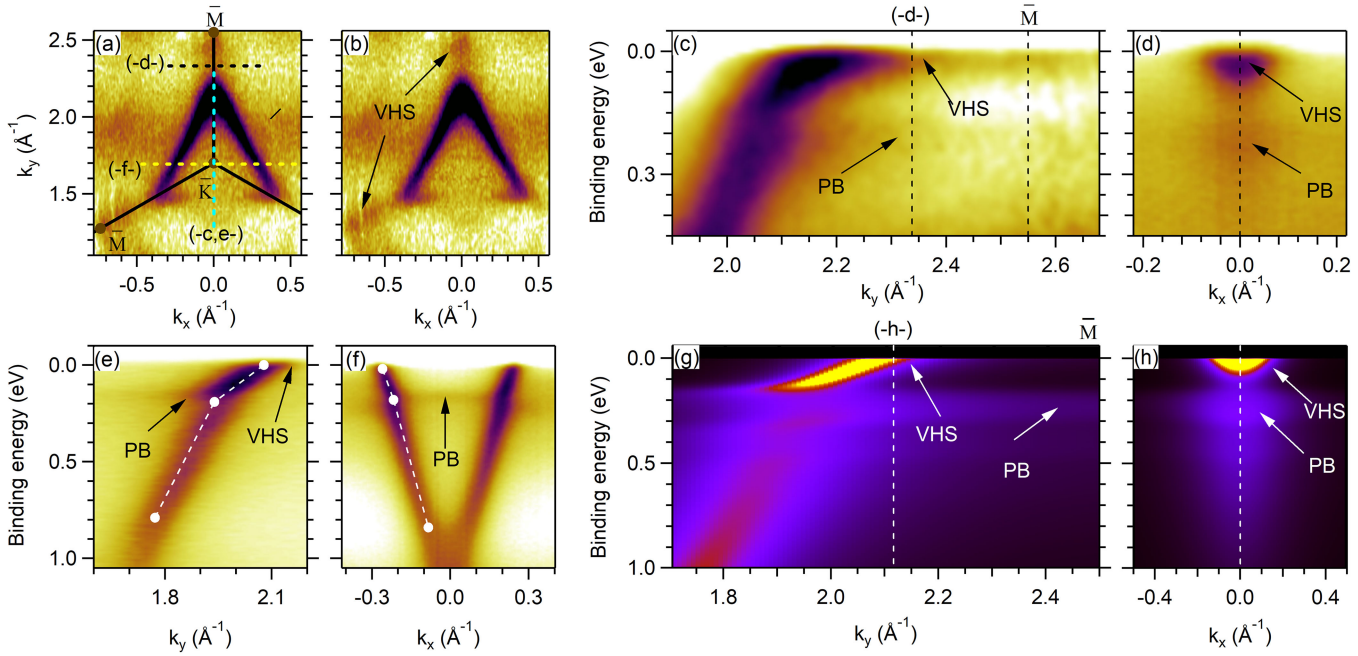

FIG. 3. (a),(b) Experimental Fermi surface of graphene/Eu/Ni(111) with and without the surface Brillouin zone on top ($h\nu = 50$ eV). (c) ARPES maps along $\bar{\mathrm{K}}\bar{\mathrm{M}}$ with an enhanced contrast ($h\nu = 40$ eV). (d) Cut perpendicular to $\bar{\Gamma}\bar{\mathrm{K}}$ direction at the point indicated by the black dashed line in (a) and (c) ($h\nu = 75$ eV). (e),(f) ARPES spectra along $\bar{\Gamma}\bar{\mathrm{K}}$ and $p(\bar{\Gamma}\bar{\mathrm{K}})$ showing the enlargement of the vicinity of the PB, white dashed lines indicate the slope of the π^* band in the proximity of the kink ($h\nu = 50$ eV). (g),(h) Theoretical simulations of the ARPES spectral function along the same cuts as in (c) and (d) including the many-body effects of the retarded electron-phonon self-energy. The binding energy scale is referred to the FL.

a strong e-ph coupling in the polaronic regime [4,56], boosted by the closeness of the VHS. Our findings support this view: in Fig. 3(d) the main spectral feature at low energy $\omega \approx 0$ associated with the VHS is accompanied by a weak replica at $\omega \approx 160$–180 meV, where no DFT bands are expected, with the typical profile of a polaronic replica [56,66] (see Fig. S5 of Supplemental Material Sec. III [31]). We confirm the robustness of this interpretation by performing many-body self-consistent calculations of the retarded e-ph self-energy in the strong-coupling regime (see Sec. III of Supplemental Material [31] for details). From the ratio of the low- and high-energy slopes [see Figs. 3(e) and 3(f)], we estimate $\lambda = 1.63$ and $\lambda = 0.3$ along $\bar{\Gamma}\bar{\mathrm{K}}$ and $p(\bar{\Gamma}\bar{\mathrm{K}})$, respectively. The resulting spectral features along $\bar{\Gamma}\bar{\mathrm{K}}$ and $p(\bar{\Gamma}\bar{\mathrm{K}})$, are shown in Figs. 3(g) and 3(h). The so-extended observed polaronic band is well reproduced when the VHS is placed in the proximity of the FL. The result of the model, using the same strength of e-ph coupling but with the VHS far from the FL, leads to a much weaker PB (see Fig. S6 and Sec. III of Supplemental Material [31]). This demonstrates a direct relation of PB to the VHS band at FL and hence to the large n doping induced by Eu.

The above reported large and spin-dependent graphene gap can give rise to a number of effects for spintronic applications, such as spin filtering, spin-selective injections, or the quantum anomalous Hall effect. Regarding the latter, we evaluated the topological character of the gap by calculating the Berry curvature [67,68] of a $(\sqrt{3} \times \sqrt{3})R30°$ Eu in contact with freestanding graphene [see Fig. S1(c) of Supplemental Material Sec. I [31]]. Figure 4(a) shows the Berry curvature $\Omega^z{}_n$ [69] as a function of binding energy and wave vector in the proximity of the Dirac cone, for the in-plane spin polarization, corresponding to the present experimental case. We can observe a finite Berry curvature that gives rise to a sizable k-resolved integral curvature [Fig. 4(b)]. Higher values can be obtained for the out-of-plane spin-polarization direction [Figs. 4(c) and 4(d)] that can be experimentally realized, for example, on a thin Co substrate [70]. Because of the $(\sqrt{3} \times \sqrt{3})R30°$ reconstruction, there is an overlap of the Dirac cone with the Eu sp states and a superposition of two opposite contributions from $\bar{\mathrm{K}}$ and $\bar{\mathrm{K}}'$ leading to a lowering of the integral curvature. In order to cross-check our findings, we also analyzed the (2×2) graphene/Eu system [Fig. S7(a) of Supplemental Material Sec. IV [31]], which can be realized on Ir(111) [28]. The disentanglement of the contributions from $\bar{\mathrm{K}}$, $\bar{\mathrm{K}}'$, and Eu sp band provides a simpler electronic pattern in the proximity of the Dirac point and leads to an increase of the Berry curvature values by orders of magnitude [Figs. S7(b) and S7(c) of Supplemental Material Sec. IV [31]]. For this system, we also calculated the anomalous Hall conductivity and found that it reaches about $-e^2/h$ at the minority gap

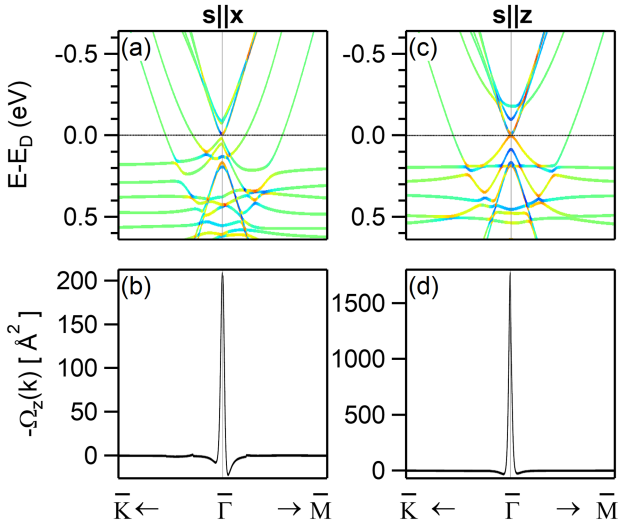

FIG. 4. Berry curvature calculation. (a) k-resolved Berry curvature for the graphene/Eu system with in-plane spin direction in the proximity of the Dirac cone along the $\bar{K}\,\bar{\Gamma}\,\bar{M}$ direction. The energy scale is referred to the Dirac point. The color scale is logarithmic: red, positive; green, zero; blue, negative. (b) Band-integrated k-resolved Berry curvature, taken on the valence states. (c),(d) same as (a),(b) for an out-of-plane spin direction.

(Fig. S8 of Supplemental Material Sec. IV [31], red arrows). This finding, according to the literature [68,71,72], elucidates the possibility of turning the graphene-Eu heterostructures into candidate systems for the quantum anomalous Hall effect.

In conclusion, through theoretical studies and experimental evidence, we show that graphene on a magnetic Eu presents an almost unaltered dispersion of the $\pi\pi^*$ states together with a lifting of spin degeneracy and a large electron doping. DFT predicts that, at the Dirac point, a large energy gap opens for the minority-spin channel due to the spin-dependent interaction with Eu $4f$ states, while in the opposite spin channel, which is undisturbed by substrate states, a smaller gap opens. ARPES and spin-ARPES data provide experimental evidence for this spin-polarized gap. We furthermore report on the spectroscopic signature of a polaronic band and demonstrate its direct relation to the large Eu-induced n doping and the VHS. A finite Berry curvature across the gap and the breaking of the time-reversal symmetry allow for the emergence of a quantum anomalous Hall effect in this system.

G. B. and N. A. gratefully acknowledge the computing time granted by the JARA Vergabegremium and provided on the JARA Partition part of the supercomputer JURECA at Forschungszentrum Jülich. N. A. acknowledges DFG support within CRC1238, Project No. 277146874-CRC 1238 (subproject C01). E. C. acknowledges financial support from PNRR MUR Project No. PE0000023-NQSTI. A. K. K. received funding from the U.S. Department of Energy, Office of Basic Energy Sciences, Contract No. DE-SC0012704 and acknowledges a receipt of a ICTP-TRIL fellowship programme from Abdus Salam International Centre for Theoretical Physics (ICTP). Authors acknowledge Elettra Sincrotrone Trieste for providing access to its synchrotron radiation facilities and for financial support under the SUI internal project and EUROFEL-ROADMAP ESFRI of the Italian Ministry of University and Research. This work has been partly performed in the framework of the nanoscience foundry and fine analysis (NFFA-MUR Italy Progetti Internazionali) facility.

*polina.sheverdyaeva@ism.cnr.it
†luisa.ferrari@ism.cnr.it

[1] N. Tombros, C. Jozsa, M. Popinciuc, H. T. Jonkman, and B. J. van Wees, Electronic spin transport and spin precession in single graphene layers at room temperature, Nature (London) **448**, 571 (2007).
[2] T. Maassen, J. J. van Den Berg, N. Ijbema, F. Fromm, T. Seyller, R. Yakimova, and B. J. van Wees, Long spin relaxation times in wafer scale epitaxial graphene on SiC(0001), Nano Lett. **12**, 1498 (2012).
[3] L. van Hove, The occurrence of singularities in the elastic frequency distribution of a crystal, Phys. Rev. **89**, 1189 (1953).
[4] J. L. McChesney, A. Bostwick, T. Ohta, T. Seyller, K. Horn, J. González, and E. Rotenberg, Extended van Hove singularity and superconducting instability in doped graphene, Phys. Rev. Lett. **104**, 136803 (2010).
[5] K. S. Novoselov, A. K. Geim, S. V. Morozov, D. Jiang, M. I. Katsnelson, I. V. Grigorieva, S. V. Dubonos, and A. A. Firsov, Two-dimensional gas of massless Dirac fermions in graphene, Nature (London) **438**, 197 (2005).
[6] A. K. Geim and K. S. Novoselov, The rise of graphene, Nat. Mater. **6**, 183 (2007).
[7] A. H. Castro Neto, F. Guinea, N. M. R. Peres, K. S. Novoselov, and A. K. Geim, The electronic properties of graphene, Rev. Mod. Phys. **81**, 109 (2009).
[8] D. Pacilé, S. Lisi, I. Di Bernardo, M. Papagno, L. Ferrari, M. Pisarra, M. Caputo, S. K. Mahatha, P. M. Sheverdyaeva, P. Moras, P. Lacovig, S. Lizzit, A. Baraldi, M. G. Betti, and C. Carbone, Electronic structure of graphene/Co interfaces, Phys. Rev. B **90**, 195446 (2014).
[9] A. Varykhalov, J. Sánchez-Barriga, A. M. Shikin, C. Biswas, E. Vescovo, A. Rybkin, D. Marchenko, and O. Rader, Electronic and magnetic properties of quasifreestanding graphene on Ni, Phys. Rev. Lett. **101**, 157601 (2008).
[10] A. Varykhalov and O. Rader, Graphene grown on Co(0001) films and islands: Electronic structure and its precise magnetization dependence, Phys. Rev. B **80**, 035437 (2009).
[11] M. Jugovac, C. Tresca, I. Cojocariu, G. Di Santo, W. Zhao, L. Petaccia, P. Moras, G. Profeta, and F. Bisti, Clarifying the apparent flattening of the graphene band near the van Hove singularity, Phys. Rev. B **105**, L241107 (2022).
[12] K. S. Novoselov, V. I. Fal'ko, L. Colombo, P. R. Gellert, M. G. Schwab, and K. Kim, A roadmap for graphene, Nature (London) **490**, 192 (2012).

[13] Y. G. Semenov, K. W. Kim, and J. M. Zavada, Spin field effect transistor with a graphene channel, Appl. Phys. Lett. **91**, 153105 (2007).
[14] E. W. Hill, F. Schedin, and P. Blake, Graphene spin valve devices, IEEE Trans. Magn. **42**, 2694 (2006).
[15] B. Zhou, X. Chen, H. Wang, K.-H. Ding, and G. Zhou, Magnetotransport and current-induced spin transfer torque in a ferromagnetically contacted graphene, J. Phys. Condens. Matter **22**, 445302 (2010).
[16] Z. Liu, F. Liu, and Y.-S. Wu, Exotic electronic states in the world of flat bands: From theory to material, Chin. Phys. B **23**, 077308 (2014).
[17] K. Sun, Z. Gu, H. Katsura, and S. Das Sarma, Nearly flatbands with nontrivial topology, Phys. Rev. Lett. **106**, 236803 (2011).
[18] M. Kang, S. Fang, L. Ye, H. C. Po, J. Denlinger, C. Jozwiak, A. Bostwick, E. Rotenberg, E. Kaxiras, J. G. Checkelsky, and R. Comin, Topological flat bands in frustrated kagome lattice CoSn, Nat. Commun. **11**, 4004 (2020).
[19] M. Jugovac, I. Cojocariu, J. Sánchez-Barriga, P. Gargiani, M. Valvidares, V. Feyer, S. Blügel, G. Bihlmayer, and P. Perna, Inducing single spin-polarized flat bands in monolayer graphene, Adv. Mater. **35**, 2301441 (2023).
[20] E. N. Voloshina and Y. S. Dedkov, Electronic and magnetic properties of the graphene/Eu/Ni(111) hybrid system, Z. Naturforsch. A **69**, 297 (2014).
[21] F. Huttmann, D. Klar, N. Atodiresei, C. Schmitz-Antoniak, A. Smekhova, A. J. Martínez-Galera, V. Caciuc, G. Bihlmayer, S. Blügel, T. Michely, and H. Wende, Magnetism in a graphene-4f − 3d hybrid system, Phys. Rev. B **95**, 075427 (2017).
[22] M. Weser, E. Voloshina, K. Horn, and Y. S. Dedkov, Electronic structure and magnetic properties of the graphene/Fe/Ni(111) intercalation-like system, Phys. Chem. Chem. Phys. **13**, 7534 (2011).
[23] E. Voloshina, A. Generalov, M. Weser, S. Böttcher, K. Horn, and Y. S. Dedkov, Structural and electronic properties of the graphene/Al/Ni(111) intercalation system, New J. Phys. **13**, 113028 (2011).
[24] A. Grüneis and D. V. Vyalikh, Tunable hybridization between electronic states of graphene and a metal surface, Phys. Rev. B **77**, 193401 (2008).
[25] O. Vilkov, A. Fedorov, D. Usachov, L. Yashina, A. Generalov, K. Borygina, N. Verbitskiy, A. Grüneis, and D. Vyalikh, Controlled assembly of graphene-capped nickel, cobalt and iron silicides, Sci. Rep. **3**, 2168 (2013).
[26] Y. S. Park, J. H. Park, H. N. Hwang, T. S. Laishram, K. S. Kim, M. H. Kang, and C. C. Hwang, Quasi-free-standing graphene monolayer on a Ni crystal through spontaneous Na intercalation, Phys. Rev. X **4**, 031016 (2014).
[27] Y. Dedkov, W. Klesse, A. Becker, F. Spaeth, C. Papp, and E. Voloshina, Decoupling of graphene from Ni(111) via formation of an interfacial NiO layer, Carbon **121**, 10 (2017).
[28] S. Schumacher, F. Huttmann, M. Petrović, C. Witt, D. F. Förster, C. Vo-Van, J. Coraux, A. J. Martínez-Galera, V. Sessi, I. Vergara, R. Rückamp, M. Grüninger, N. Schleheck, F. Meyer zu Heringdorf, P. Ohresser, M. Kralj, T. O. Wehling, and T. Michely, Europium underneath graphene on Ir(111): Intercalation mechanism, magnetism, and band structure, Phys. Rev. B **90**, 235437 (2014).
[29] C. L. Kane and E. J. Mele, Quantum spin Hall effect in graphene, Phys. Rev. Lett. **95**, 226801 (2005).
[30] N. Fläschner, B. S. Rem, M. Tarnowski, D. Vogel, D.-S. Lühmann, K. Sengstock, and C. Weitenberg, Experimental reconstruction of the Berry curvature in a Floquet Bloch band, Science **352**, 1091 (2016).
[31] See Supplemental Material at http://link.aps.org/supplemental/10.1103/PhysRevLett.132.266401, which includes Refs. [32–52], for additional information about the experimental methods and a detailed discussion of the numerical simulations.
[32] J. P. Perdew, K. Burke, and M. Ernzerhof, Generalized gradient approximation made simple, Phys. Rev. Lett. **77**, 3865 (1996).
[33] K. Lee, E. D. Murray, L. Kong, B. I. Lundqvist, and D. C. Langreth, Higher-accuracy van der Waals density functional, Phys. Rev. B **82**, 081101(R) (2010).
[34] A. D. Becke, Density functional calculations of molecular bond energies, J. Chem. Phys. **84**, 4524 (1986).
[35] I. Hamada, van der Waals density functional made accurate, Phys. Rev. B **89**, 121103(R) (2014).
[36] D. Wortmann, G. Michalicek, R. Hilgers, A. Neukirchen, H. Janssen, U. Grytsiuk, J. Broeder, and C.-R. Gerhorst, Fleur, 2023, 10.5281/zenodo.7778444.
[37] Y. Ren, X. Deng, Z. Qiao, C. Li, J. Jung, C. Zeng, Z. Zhang, and Q. Niu, Single-valley engineering in graphene superlattices, Phys. Rev. B **91**, 245415 (2015).
[38] C. Chen, J. Avila, S. Wang, Y. Wang, M. Mucha-Kruczyński, C. Shen, R. Yang, B. Nosarzewski, T. P. Devereaux, G. Zhang, and M. C. Asensio, Emergence of interfacial polarons from electron–phonon coupling in graphene/h-BN van der Waals heterostructures, Nano Lett. **18**, 1082 (2018).
[39] C. Chen *et al.*, Strong inter-valley electron-phonon coupling in magic-angle twisted bilayer graphene, arXiv:2303.14903.
[40] F. Marsiglio, M. Schossmann, and J. P. Carbotte, Iterative analytic continuation of the electron self-energy to the real axis, Phys. Rev. B **37**, 4965 (1988).
[41] G. M. Eliashberg, Interactions between electrons and lattice vibrations in a superconductor, Sov. Phys. JETP **11**, 696 (1960), http://jetp.ras.ru/cgi-bin/r/index/e/11/3/p696?a=list.
[42] G. Grimvall, *The Electron-Phonon Interaction in Metals* (North-Holland, Amsterdam, 1981).
[43] D. J. Scalapino, The electron-phonon interaction and strong-coupling superconductors, in *Superconductivity*, edited by R. D. Parks (Dekker, New York, 1969), p. 449, 10.1201/9780203737965.
[44] A. Lanzara, P. Bogdanov, X. Zhou, S. Kellar, D. Feng, E. Lu, T. Yoshida, H. Eisaki, A. Fujimori, K. Kishio, J. Shimoyama, T. Noda, S. Uchida, Z. Hussain, and Z. Shen, Evidence for ubiquitous strong electron–phonon coupling in high-temperature superconductors, Nature (London) **412**, 510 (2001).
[45] F. Mazzola, J. W. Wells, R. Yakimova, S. Ulstrup, J. A. Miwa, R. Balog, M. Bianchi, M. Leandersson, J. Adell, P. Hofmann, and T. Balasubramanian, Kinks in the σ band of graphene induced by electron-phonon coupling, Phys. Rev. Lett. **111**, 216806 (2013).

[46] S. Engelsberg and J. R. Schrieffer, Coupled electron-phonon system, Phys. Rev. **131**, 993 (1963).
[47] E. Cappelluti and L. Pietronero, Electron-phonon renormalization in small Fermi energy systems, Phys. Rev. B **68**, 224511 (2003).
[48] A. Knigavko, J. P. Carbotte, and F. Marsiglio, Observation of phonon structure in electron density of states of a normal metal, Europhys. Lett. **71**, 776 (2005).
[49] G. D. Mahan, *Many Particle Physics* (Springer, New York, NY, 2000), 10.1007/978-1-4757-5714-9.
[50] I. G. Lang and Yu. A. Firsov, Kinetic theory of semiconductors with low mobility, Sov. Phys. JETP **16**, 1301 (1963), http://www.jetp.ras.ru/cgi-bin/e/index/e/16/5/p1301?a=list.
[51] S. Ciuchi, F. de Pasquale, S. Fratini, and D. Feinberg, Dynamical mean-field theory of the small polaron, Phys. Rev. B **56**, 4494 (1997).
[52] P. C. Pattnaik, C. L. Kane, D. M. Newns, and C. C. Tsuei, Evidence for the van Hove scenario in high-temperature superconductivity from quasiparticle-lifetime broadening, Phys. Rev. B **45**, 5714 (1992).
[53] I. I. Klimovskikh, M. M. Otrokov, V. Y. Voroshnin, D. Sostina, L. Petaccia, G. Di Santo, S. Thakur, E. V. Chulkov, and A. M. Shikin, Spin–orbit coupling induced gap in graphene on Pt(111) with intercalated Pb monolayer, ACS Nano **11**, 368 (2017).
[54] S. Sung, S. Kim, P. Lee, J. Kim, M. Ryu, H. Park, K. Kim, B. I. Min, and J. Chung, Observation of variable hybridized-band gaps in Eu-intercalated graphene, Nanotechnology **28**, 205201 (2017).
[55] L. Daukiya, M. N. Nair, S. Hajjar-Garreau, F. Vonau, D. Aubel, J. L. Bubendorff, M. Cranney, E. Denys, A. Florentin, G. Reiter, and L. Simon, Highly *n*-doped graphene generated through intercalated terbium atoms, Phys. Rev. B **97**, 035309 (2018).
[56] S. Link, S. Forti, A. Stöhr, K. Küster, M. Rösner, D. Hirschmeier, C. Chen, J. Avila, M. C. Asensio, A. A. Zakharov, T. O. Wehling, A. I. Lichtenstein, M. I. Katsnelson, and U. Starke, Introducing strong correlation effects into graphene by gadolinium intercalation, Phys. Rev. B **100**, 121407(R) (2019).
[57] P. Rosenzweig, H. Karakachian, S. Link, K. Muller, and U. Starke, Tuning the doping level of graphene in the vicinity of the Van Hove singularity via ytterbium intercalation, Phys. Rev. B **100**, 035445 (2019).
[58] M. Papagno, S. Rusponi, P. M. Sheverdyaeva, S. Vlaic, M. Etzkorn, D. Pacilé, P. Moras, C. Carbone, and H. Brune, Large band gap opening between graphene Dirac cones induced by Na adsorption onto an Ir superlattice, ACS Nano **6**, 199 (2012).
[59] D. Pacilé, P. Leicht, M. Papagno, P. M. Sheverdyaeva, P. Moras, C. Carbone, K. Krausert, L. Zielke, M. Fonin, Y. S. Dedkov, F. Mittendorfer, J. Doppler, A. Garhofer, and J. Redinger, Artificially lattice-mismatched graphene/metal interface: Graphene/Ni/Ir(111), Phys. Rev. B **87**, 035420 (2013).
[60] N. Ehlen, M. Hell, G. Marini, E. H. Hasdeo, R. Saito, Y. Falke, M. O. Goerbig, G. Di Santo, L. Petaccia, G. Profeta, and A. Grüneis, Origin of the flat band in heavily Cs-doped graphene, ACS Nano **14**, 1055 (2020).
[61] A. Bostwick, T. Ohta, T. Seyller, K. Horn, and E. Rotenberg, Quasiparticle dynamics in graphene, Nat. Phys. **3**, 36 (2007).
[62] A. V. Fedorov, N. I. Verbitskiy, D. Haberer, C. Struzzi, L. Petaccia, D. Usachov, O. Y. Vilkov, D. V. Vyalikh, J. Fink, M. Knupfer, B. Büchner, and A. Grüneis, Observation of a universal donor-dependent vibrational mode in graphene, Nat. Commun. **5**, 3257 (2014).
[63] D. Haberer, L. Petaccia, A. V. Fedorov, C. S. Praveen, S. Fabris, S. Piccinin, O. Vilkov, D. V. Vyalikh, A. Preobrajenski, N. I. Verbitskiy, H. Shiozawa, J. Fink, M. Knupfer, B. Büchner, and A. Grüneis, Anisotropic Eliashberg function and electron-phonon coupling in doped graphene, Phys. Rev. B **88**, 081401(R) (2013).
[64] S. Ichinokura, M. Toyoda, M. Hashizume, K. Horii, S. Kusaka, S. Ideta, K. Tanaka, R. Shimizu, T. Hitosugi, S. Saito, and T. Hirahara, Van Hove singularity and Lifshitz transition in thickness-controlled Li-intercalated graphene, Phys. Rev. B **105**, 235307 (2022).
[65] P. Rosenzweig, H. Karakachian, D. Marchenko, K. Küster, and U. Starke, Overdoping graphene beyond the van Hove singularity, Phys. Rev. Lett. **125**, 176403 (2020).
[66] J. M. Riley, F. Caruso, C. Verdi, L. B. Duffi, M. D. Watson, L. Bawden, K. Volckaert, G. van der Laan, T. Hesjedal, M. Hoesch, F. Giustino, and P. D. C. King, Crossover from lattice to plasmonic polarons of a spin-polarised electron gas in ferromagnetic EuO, Nat. Commun. **9**, 2305 (2018).
[67] A. G. Rybkin, A. V. Tarasov, A. A. Rybkina, D. Y. Usachov, A. E. Petukhov, A. V. Eryzhenkov, D. A. Pudikov, A. A. Gogina, I. I. Klimovskikh, G. Di Santo, L. Petaccia, A. Varykhalov, and A. M. Shikin, Sublattice ferrimagnetism in quasifreestanding graphene, Phys. Rev. Lett. **129**, 226401 (2022).
[68] Z. Zanolli, C. Niu, G. Bihlmayer, Y. Mokrousov, P. Mavropoulos, M. J. Verstraete, and S. Blügel, Hybrid quantum anomalous Hall effect at graphene-oxide interfaces, Phys. Rev. B **98**, 155404 (2018).
[69] J. Qiao, J. Zhou, Z. Yuan, and W. Zhao, Calculation of intrinsic spin Hall conductivity by Wannier interpolation, Phys. Rev. B **98**, 214402 (2018).
[70] N. Rougemaille, A. Ndiaye, J. Coraux, C. Vo-Van, O. Fruchart, and A. Schmid, Perpendicular magnetic anisotropy of cobalt films intercalated under graphene, Appl. Phys. Lett. **101**, 142403 (2012).
[71] Z. Qiao, S. A. Yang, W. Feng, W.-K. Tse, J. Ding, Y. Yao, J. Wang, and Q. Niu, Quantum anomalous Hall effect in graphene from Rashba and exchange effects, Phys. Rev. B **82**, 161414(R) (2010).
[72] Y. Han, Z. Yan, Z. Li, X. Xu, Z. Zhang, Q. Niu, and Z. Qiao, Large Rashba spin-orbit coupling and high-temperature quantum anomalous Hall effect in Re-intercalated graphene/CrI_3 heterostructure, Phys. Rev. B **107**, 205412 (2023).